JACS
JOURNAL OF THE AMERICAN CHEMICAL SOCIETY

ARTICLE

pubs.acs.org/JACS

Alkaline-Alkaline Earth Fluoride Carbonate Crystals $ABCO_3F$ (A = K, Rb, Cs; B = Ca, Sr, Ba) as Nonlinear Optical Materials

Guohong Zou, Ning Ye,* Ling Huang, and Xinsong Lin

Key Laboratory of Optoelectronic Materials Chemistry and Physics, Fujian Institute of Research on the Structure of Matter, Chinese Academy of Sciences, Fuzhou, Fujian, 350002, P. R. China

Supporting Information

ABSTRACT: A new series of alkaline−alkaline earth fluoride carbonates ($KSrCO_3F$, $RbSrCO_3F$, $KCaCO_3F$, $RbCaCO_3F$, $CsCaCO_3F$, and $Cs_3Ba_4(CO_3)_3F_5$) were synthesized by spontaneous crystallization with molten fluxes. Their crystal structures, except for $Cs_3Ba_4(CO_3)_3F_5$, exhibit the stacking of $[AF]_\infty$ (A = K, Rb, Cs) and $[B(CO_3)]_\infty$ (B = Ca, Sr) layers, and the coplanar alignment of $[CO_3]$ triangles. The results from the UV−vis diffuse reflectance spectroscopy study of the powder samples indicated that the short-wavelength absorption edges were all below 200 nm, except for $Cs_3Ba_4(CO_3)_3F_5$, which is about 210 nm. Second-harmonic generation (SHG) on polycrystalline samples was measured using the Kurtz and Perry technique, which indicated that these carbonates are all phase-matchable materials in both visible and the UV region, and their measured SHG coefficients were about 3.33, 3.33, 3.61, 1.11, 1.11, and 1.20 times as large as that of d_{36} (KDP), respectively.

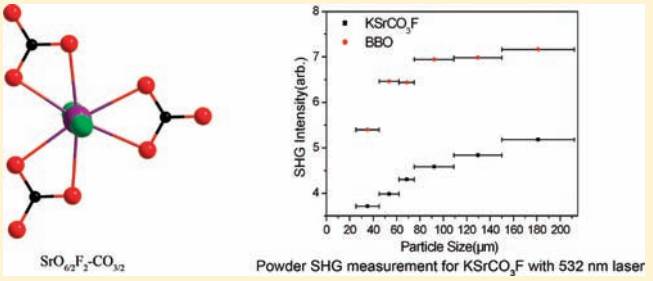

1. INTRODUCTION

Ultraviolet (UV) nonlinear optical (NLO) crystals[1−11] that can produce UV coherent light, which is considered as a clean energy source for the synthesis and processing of materials, have played an important role in laser science and technology. The search for new NLO materials[12−16] with high NLO coefficients and wide UV transparency has attracted considerable attention. Currently, most of the UV NLO crystals reported are borate crystals.[17−19] On the basis of the anionic groups, there are four main basic structure units in these borates crystals. The following are examples: β-BaB_2O_4 (BBO)[20] with the anionic groups $[B_3O_6]^{3-}$; LiB_3O_5,[21] CsB_3O_5[22] and $CsLiB_6O_{10}$[23,24] with $[B_3O_7]^{5-}$; $KBe_2BO_3F_2$,[25] $Sr_2Be_2B_2O_7$,[6] $K_2Al_2B_2O_7$[26] with $[BO_3]^{3-}$; $Li_2B_4O_7$[27] with $[B_4O_9]^{6-}$. Among these, the planar $[BO_3]^{3-}$ anionic group, having a moderate birefringence and a large microscopic second-order susceptibility $\beta^{(2)}$, is the most suitable basic structural unit of NLO crystals for UV and deep-UV light generation. The only other inorganic anionic groups with a π-conjugated system and a planar triangle structure as $[BO_3]^{3-}$ are $[CO_3]^{2-}$ and $[NO_3]^-$. However, most nitrates dissolve easily in water and would not be suitable for industrial applications. Although some carbonates are stable in air, especially those that do not contain alkali metals, it is difficult to grow the single crystals because the carbonates decompose at high temperature. To obtain novel NLO crystals with low melting point, we introduced alkaline fluoride into carbonates to form complex salts and synthesized a family of fluoride carbonates.

Fluoride carbonates[28] have been known to occur mainly in natural minerals. An intense second harmonic generation (SHG) signal was observed in $K_4RE_2(CO_3)_3F_4$[29] (RE = Nd, Sm, Eu, Gd), but large single crystals could not be grown. Some transition metal fluoride carbonates[30−34] such as $KCu(CO_3)F$[31] and $BaM(CO_3)F_2$ (M = Mn, Cu, Zn)[30] and rare earths fluoride carbonates[35−37] have been crystallized in subcritical and supercritical hydrothermal conditions. Only one phase, $KCa(CO_3)F$,[38,39] has been synthesized by solid-state reaction, but attempts at growing the single crystals had failed. However, the properties of these NLO carbonates have not been fully investigated. Similar to borates containing $[BO_3]$, the optimal arrangement of the $[CO_3]$ groups for large NLO effect is the coplanar and parallel alignment of $[CO_3]$ groups. From the structural analysis of known fluoride carbonates,[30,38,39] it was found that polygonal bipyramid coordination of the countercations with equatorial M−O bonds, such as MO_3F_2 or MO_6F_2 groups, results in a coplanar alignment of the $[CO_3]$ groups in the lattice. Therefore, choice of suitable cations is critical in the structural design of noncentrosymmetric (NCS) fluoride carbonates. To ensure high transmission in the UV region, alkali and alkaline earth metals were chosen as the countercations for the systematic synthesis of UV NLO crystals based on the A_2CO_3−BCO_3−BF_2 (A = K, Rb, Cs; B = Ca, Sr, Ba) system. A new series of alkaline−alkaline earth fluoride carbonates (i.e., $KSrCO_3F$, $RbSrCO_3F$, $RbCaCO_3F$, $CsCaCO_3F$, and $Cs_3Ba_4(CO_3)_3F_5$) were synthesized by spontaneous crystallization with molten fluxes, and we also grew the single crystals of $KCaCO_3F$. All of the six crystals are NCS.[40,41] All these crystals, except for $Cs_3Ba_4(CO_3)_3F_5$, consist of infinite B−F−B (B = Ca, Sr) chains parallel to the c-axis and planar $[CO_3]$ group perpendicular to

Received: October 2, 2011
Published: October 28, 2011

Table 1. Crystal Data and Structure Refinement for $KSrCO_3F$, $RbSrCO_3F$, $KCaCO_3F$, $RbCaCO_3F$, $CsCaCO_3F$, and $Cs_3Ba_4(CO_3)_3F_5$[a]

formula	$KSrCO_3F$	$RbSrCO_3F$	$KCaCO_3F$	$RbCaCO_3F$	$CsCaCO_3F$	$Cs_3Ba_4(CO_3)_3F_5$
formula mass (amu)	205.73	252.10	158.19	204.56	252.00	1223.12
crystal system	hexagonal	hexagonal	hexagonal	hexagonal	hexagonal	hexagonal
space group	$P\bar{6}m2$	$P\bar{6}m2$	$P\bar{6}m2$	$P\bar{6}2m$	$P\bar{6}2m$	$P6_3mc$
a (Å)	5.2598(5)	5.3000(4)	5.0968(6)	9.1979(6)	9.2999(4)	11.5158(9)
c (Å)	4.6956(11	4.7900(6)	4.4553(7)	4.4463(6)	4.5400(3)	7.6132(12)
α (deg)	90	90	90	90	90	90
γ (deg)	120	120	120	120	120	120
V(Å^3)	112.50(3)	116.525(19)	100.23(2)	325.77(5)	340.05(3)	874.35(17)
Z	1	1	1	3	3	2
ρ(calcd)(g/cm^3)	3.037	3.137	2.621	3.128	3.692	4.646
temp (K)	293(2)	293(2)	293(2)	293(2)	293(2)	293(2)
λ (Å)	0.71073	0.71073	0.71073	0.71073	0.71073	0.71073
F(000)	96	98	78	288	342	1048
μ (mm^{-1})	12.809	21.794	2.495	12.479	9.202	15.125
θ (deg)	4.34−27.43	4.25−27.37	4.57−27.08	4.43−27.37	2.53−27.47	2.04−27.42
index range	$-6 \le h \le 6$	$-6 \le h \le 6$	$-6 \le h \le 6$	$-11 \le h \le 11$	$-12 \le h \le 11$	$-14 \le h \le 14$
	$-5 \le h \le 6$	$-6 \le h \le 6$	$-6 \le h \le 5$	$-11 \le h \le 11$	$-12 \le h \le 12$	$-14 \le h \le 14$
	$-6 \le h \le 6$	$-6 \le h \le 6$	$-5 \le h \le 5$	$-5 \le h \le 5$	$-5 \le h \le 5$	$-9 \le l \le 7$
R_{int}	0.0368	0.0542	0.0173	0.0488	0.0380	0.0527
R/wR ($I > 2\sigma(I)$)	0.0152/0.0267	0.0239/0.0500	0.0108/0.0272	0.0195/0.0352	0.0182/0.0448	0.0196/0.0384
R/wR (all data)	0.0152/0.0267	0.0246/0.0501	0.0108/0.0272	0.0198/0.0353	0.0182/0.0448	0.0207/0.0441
GOF on F_2	0.891	1.071	1.261	0.976	1.329	1.170
absolute structure parameter	0.041(17)	0.00	0.04(8)	0.008(14)	0.05(5)	0.07(7)
largest diff peak and hole (e/Å^{-3})	0.270 and −0.323	0.660 and −0.359	0.129 and −0.158	0.516 and −0.547	0.765 and −1.526	0.790 and −0.960

[a] $R(F) = \Sigma||F_o| - |F_c||/\Sigma|F_o|$. $wR(F_o^2) = [\Sigma w(F_o^2 - F_c^2)^2/\Sigma w(F_o^2)^2]^{1/2}$.

the c-axis. Herein, we report the syntheses, crystal structures, thermal behaviors, spectra, NLO properties and the structure−properties relationship of these fluoride carbonates.

2. EXPERIMENTAL SECTION

2.1. Reagents. K_2CO_3(99%), Rb_2CO_3(99.5%), Cs_2CO_3(99.5%), $CaCO_3$(99%), $SrCO_3$ (99%), $BaCO_3$(99%), SrF_2(99%),CaF_2 (99%), and BaF_2 (99%) were purchased from Sinopharm and used as received.

2.2. Syntheses of $KSrCO_3F$ and $RbSrCO_3F$. Single crystals of $KSrCO_3F$ were grown from a high temperature solution by using K_2CO_3−SrF_2 as a flux. This solution was prepared in a platinum crucible by melting a mixture of K_2CO_3, $SrCO_3$, and SrF_2 at a molar ratio of $K_2CO_3/SrCO_3/SrF_2$ = 2:1:2. The mixture (10 g) was heated in a programmable temperature electric furnace at 800 °C until the melt became transparent and clear. The homogenized melt solution was then cooled rapidly (50 °C/h) to the initial crystallization temperature (700 °C). It was further cooled slowly (3 °C/h) to the final crystallization temperature (600 °C) and then allowed to cool (30 °C/h) to room temperature. The flux attached to the crystal was readily dissolved in water when the crystal was put in distilled water (50 °C) for 2 h. Under the same conditions, single crystals of $RbSrCO_3F$ were grown at a molar ratio of $Rb_2CO_3/SrCO_3/SrF_2$ = 1.5:1:1.5 by using Rb_2CO_3−SrF_2 as a flux.

2.3. Syntheses of $KCaCO_3F$, $RbCaCO_3F$, $CsCaCO_3F$, and $Cs_3Ba_4(CO_3)_3F_5$. Single crystals of $KCaCO_3F$ were grown from a high temperature solution by using K_2CO_3−CaF_2 as a flux in a CO_2 atmosphere. This solution was prepared in a platinum crucible by melting a mixture of K_2CO_3, $CaCO_3$, and CaF_2 at a molar ratio of $K_2CO_3/CaCO_3/CaF_2$ = 2:1:1.5 under a flow of CO_2 gas. The mixture (10 g) was heated in a programmable temperature electric furnace at 850 °C until the melt became transparent and clear. The homogenized melt solution was then cooled rapidly (50 °C/h) to the initial crystallization temperature (750 °C). It was further cooled slowly (3 °C/h) to the final crystallization temperature (600 °C) and then allowed to cool (30 °C/h) to room temperature. The flux attached to the crystal was readily dissolved in water when the crystal was put in distilled water (50 °C) for 2 h. Under the same conditions, single crystals of $RbCaCO_3F$ and $CsCaCO_3F$ were grown at a molar ratio of A_2CO_3 (A = Rb, Cs)/$CaCO_3$/CaF_2 = 2:1:2 by using A_2CO_3 (A = Rb, Cs)−CaF_2 as a flux. Single crystals of $Cs_3Ba_4(CO_3)_3F_5$ were grown at a molar ratio of $Cs_2CO_3/BaCO_3/BaF_2$ = 2:1.5:3.

2.4. Single Crystal X-ray Diffraction. Single crystal X-ray diffraction data were collected at room temperature on a Rigaku Mercury CCD diffractometer with graphite-monochromatic Mo Kα radiation (λ = 0.71073 Å). A transparent block of crystal was mounted on a glass fiber with epoxy for structure determination. A hemisphere of data was collected using a narrow-frame method with ω-scan mode. The data were integrated using the CrystalClear program, and the intensities were corrected for Lorentz polarization, air absorption, and absorption attributable to the variation in the path length through the detector faceplate. Absorption corrections based on the Multiscan technique were also applied. The structure was solved by the direct methods and refined by full-matrix least-squares fitting on F^2 by SHELX-97.[42] All of the structures were verified using the ADDSYM algorithm from the program PLATON,[43] and no higher symmetries were found. Relevant crystallographic data and details of the experimental conditions for $KCaCO_3F$, $KSrCO_3F$, $RbSrCO_3F$, $RbCaCO_3F$, $CsCaCO_3F$, and $Cs_3Ba_4(CO_3)_3F_5$ are summarized in Table 1. Atomic coordinates and isotropic displacement coefficients are listed in Tables S1−S6 and bond lengths in Tables S7−S12 in the Supporting Information.

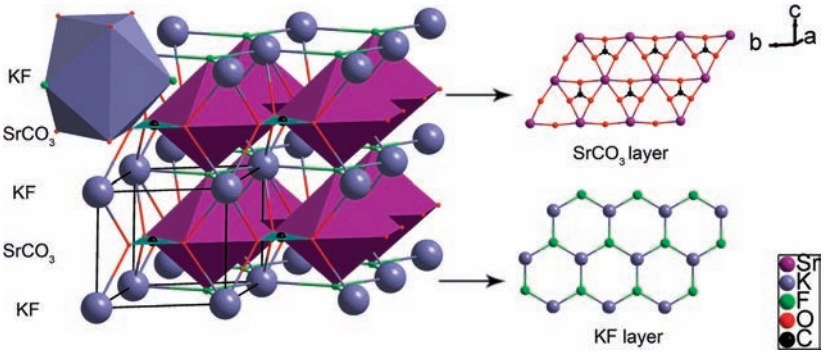

Figure 1. Crystal structure of $KSrCO_3F$.

2.5. Powder X-ray Diffraction. X-ray diffraction patterns of polycrystalline materials were obtained on a Rigaku Dmax2500 powder X-ray diffractometer by using Cu Kα radiation (λ = 1.540598 Å) at room temperature in the angular range of $2\theta = 0-60°$ with a scan step width of 0.05° and a fixed time of 0.2 s. The PXRD patterns for $KCaCO_3F$, $KSrCO_3F$, $RbSrCO_3F$, $RbCaCO_3F$, $CsCaCO_3F$, and $Cs_3Ba_4(CO_3)_3F_5$ showed good agreement with the calculated XRD patterns from the single-crystal models (see Figure S2 in the Supporting Information).

2.6. TG/DTA Analysis. The TG/DTA scans were measured on a NETZSCH STA 449C simultaneous analyzer. Reference (Al_2O_3) and crystal samples (5−15 mg) were enclosed in Al_2O_3 crucibles and heated from room temperature to 900 °C at a rate of 10 °C/min under a constant flow of nitrogen gas. The TG/DTA residues were visually inspected and then analyzed by X-ray powder diffraction after the experiments.

2.7. UV−vis Diffuse Reflectance Spectroscopy. The UV−vis diffuse reflection data were recorded at room temperature using a powder sample with $BaSO_4$ as a standard (100% reflectance) on a PerkinElmer Lamda-900 UV/vis/NIR spectrophotometer and scanned at 200−800 nm. Reflectance spectra were converted to absorbance using the Kubelka−Munk function.[44,45]

2.8. Second-Harmonic Generation. Polycrystalline second-harmonic generation (SHG) signals were measured using the method adapted from Kurtz and Perry.[46] Since SHG efficiencies are known to depend strongly on particle size, polycrystalline samples were ground and sieved into the following particle size ranges: 25−45, 45−62, 62−75, 75−109, 109−150, and 150−212 μm. The nanotrapping effects[47] which may change NLO effect were neglected because the size range in the powder SHG measurement is between 20 to 500 μm. The measurements were performed with a Q-switched Nd:YAG laser at 1064 nm and a frequency doubling at 532 nm, for visible and UV SHG, respectively. To make relevant comparisons with known NLO materials, crystalline KDP and BBO were also ground and sieved into the same particle size ranges and used as the references for visible and UV SHG, respectively. The samples were pressed between glass microscope cover slides and secured with tape in 1-mm thick aluminum holders containing an 8-mm diameter hole. They were then placed in a light-tight box and irradiated with a pulsed laser. A cutoff filter was used to limit background flash-lamp light on the sample, and an interference filter was used to select the second harmonic for detection with a photomultiplier tube attached to a RIGOL DS1052E 50-MHz oscilloscope. This procedure was then repeated using the standard nonlinear optical materials KDP and BBO, and the ratio of the second-harmonic intensity outputs was calculated. No index-matching fluid was used in any of the experiments.

3. RESULTS AND DISCUSSION

3.1. Crystal Growth and Thermal Behavior. We have successfully synthesized a new series of alkaline−alkaline earth fluoride carbonates $KSrCO_3F$, $RbSrCO_3F$, $RbCaCO_3F$, $CsCaCO_3F$, and $Cs_3Ba_4(CO_3)_3F_5$ based on the $A_2CO_3-BCO_3-BF_2$ (A = K, Rb, Cs; B = Ca, Sr, Ba) systems. Unlike the subcritical and supercritical hydrothermal crystallization of previously reported fluoride carbonates, all six carbonate crystals from this study were grown by spontaneous crystallization with molten fluxes under ambient pressure, which is feasible for industrial applications.

As shown in Figure S1, the DTA curves for $KSrCO_3F$ and $RbSrCO_3F$ exhibit only one endothermic peak at 690 and 720 °C, respectively, along with minor weight loss observed on the TGA curve due to the volatility upon melting. Analysis of the powder XRD pattern of the residues revealed that $KSrCO_3F$ and $RbSrCO_3F$ did not change all the time, demonstrating that they melt congruently. Therefore, large crystals of $KSrCO_3F$ and $RbSrCO_3F$ could be grown easily in the air.

As shown in Figure S1, the DTA curves of $ACaCO_3F$ (A = K, Rb, Cs) show one endothermic peak along with weight loss on the TGA curves at their melting points. Analysis of the powder XRD pattern of the residues revealed that $KCaCO_3F$ was decomposed into $KCaF_3$ and CaO, while $RbCaCO_3F$ into $RbCaF_3$ and CaO, and $CsCaCO_3F$ into $CsCaF_3$ and CaO, suggesting that they are incongruently melting compounds in the air. Therefore, large crystals of $ACaCO_3F$ (A = K, Rb, Cs) may be grown with a flux under a flow of CO_2.

DTA results indicate that the thermal behavior of $Cs_3Ba_4(CO_3)_3F_5$ was different because there were three endothermic peaks as the samples were being heated. The first endothermic peak at 625 °C corresponded to the phase transitions of $Cs_3Ba_4(CO_3)_3F_5$. The second endothermic peak at 665 °C and the third endothermic peak at 820 °C corresponded to the two-step incongruent melting processes associated with the decomposition of $Cs_3Ba_4(CO_3)_3F_5$ finally into BaF_2 and $BaCO_3$.

Because it is difficult to obtain fluoride carbonate crystals by high temperature solid state reaction due to carbonate decomposition, we employed spontaneous crystallization in a molten flux based on the self-fluxed system to grow the crystals. Moreover, crystals of $KCaCO_3F$, $RbCaCO_3F$, and $CsCaCO_3F$ were grown under a constant flow of CO_2 to get enough partial CO_2 pressure. The six crystals are all stable in air and not hydroscopic, except for $Cs_3Ba_4(CO_3)_3F_5$ crystals, which deliquesce slightly.

3.2. Crystal Structure. $ASrCO_3F$ (A = K, Rb) and $KCaCO_3F$ are isostructural and crystallize into a hexagonal crystal system with an acentric space group of $P\bar{6}m2$. Hence, only the structure of $KSrCO_3F$ will be discussed in detail (Figure 1). The structure of $KSrCO_3F$ can be described with KO_6F_3 and SrO_6F_2 polyhedra and CO_3 triangular entities. In the structure, the C atom is coordinated to three O atoms to form a planar CO_3 triangle with

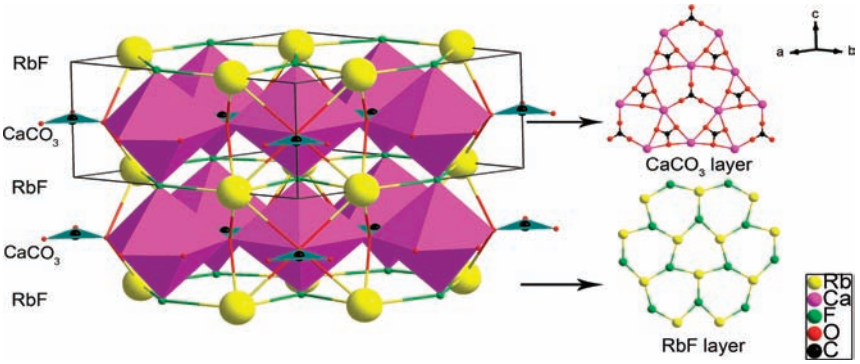

Figure 2. Crystal structure of $RbCaCO_3F$.

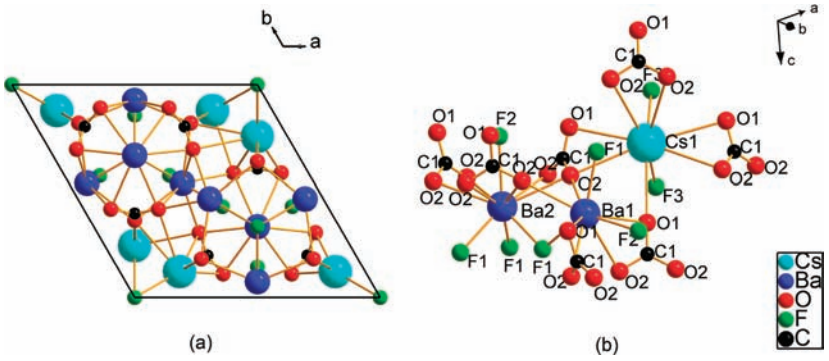

Figure 3. Crystal structure of $Cs_3Ba_4(CO_3)_3F_5$.

C−O bond lengths at 1.291(4) Å and O−C−O bond angles at 120.000(1)°. The SrO_6F_2 hexagonal bipyramid shares its six equatorial oxygen atoms with three CO_3 groups to form a flat $SrCO_3$ layer and connects adjacent layers with its apical F atoms along the *c* direction. Within a single $SrCO_3$ layer, the cooperative connection of hexagon SrO_6 and triangular CO_3 make all CO_3 groups aligned parallel in the *a*−*b* plane, giving the maximum contribution to a large macroscopic SHG effect.[48] The K ions were located in the cavities of the three-dimensional (3D) network and exhibit a tricapped trigonal prism coordination. All K and the F ions were located in the same layer between the $SrCO_3$ layers.

$RbCaCO_3F$ and $CsCaCO_3F$ are isostructural and crystallize into a hexagonal crystal system with an acentric space group of $P\bar{6}2m$. Hence, only the structure of $RbCaCO_3F$ will be discussed in detail. As shown in Figure 2, the C atoms are coordinated to three O atoms to form planar $[CO_3]$ triangles with C−O bond lengths ranging from 1.276(5) to 1.298(3) Å and O−C−O bond angles at 120.000(1)°. The structure is made up of alternately stacked layers of $[Ca(CO_3)]_\infty$ and $[RbF]_\infty$, and all the adjacent layers are connected by infinite Ca−F−Ca chains parallel to the *c*-axis, forming a three-dimensional network similar to that of $KSrCO_3F$. However, the Ca atom is 7-fold coordinated, forming a $[CaO_5F_2]$ pentagonal bipyramid which is connected to three CO_3 groups by sharing its five equatorial oxygen atoms. Within a single $CaCO_3$ layer, one-third of the three CO_3 groups is aligned antiparallel to the other two, making only one-third of contribution to the SHG coefficients.

$Cs_3Ba_4(CO_3)_3F_5$ crystallizes into a hexagonal crystal system with an acentric space group of $P6_3mc$, which is illustrated along the *c*-axis in Figure 3a. The structure is an intricate three-dimensional framework of interconnecting Ba-centered polyhedra, Cs-centered polyhedra, and isolated CO_3 triangles. The cesium atom is surrounded by seven oxygen atoms (three O(1) and four O(2)) and two F(3) atoms, forming a CsO_7F_2 polyhedron. The barium atom possesses two distinctive coordination environments. The Ba(1) atom is surrounded by six oxygen atoms (two O(1) and four O(2)) and three fluorine atoms (two F(1) and one F(2)), forming a BaO_6F_3 polyhedron. The Ba(2) atom is surrounded by six oxygen (O(2)) atoms and four F atoms (three F(1) and one F(2)), forming a BaO_6F_4 polyhedron. The C atoms are coordinated to three O atoms to form planar $[CO_3]$ triangles with C−O bond lengths ranging from 1.276(5) to 1.298(3) Å and O−C−O bond angles at about 120°. The network is constructed with Ba- and Cs-centered polyhedra and the $[CO_3]$ triangles by sharing their edges or faces. Unlike the carbonates described formerly, these $[CO_3]$ triangles are not coplanar aligned.

The bond valence sums for $KSrCO_3F$, $RbSrCO_3F$, $KCaCO_3F$ $RbCaCO_3F$, $CsCaCO_3F$, and $Cs_3Ba_4(CO_3)_3F_5$ are calculated using the formula

$$V_i = \sum_j S_{ij} = \sum_j \exp\{(r_0 - r_{ij})/B\} \quad (1)$$

where S_{ij} is the bond valence associated with bond length r_{ij} and r_0 and B (usually 0.37) are empirically determined parameters.[49,50] The calculated total bond valence for K, Rb, Cs, Ca, Sr, Ba, C, O and F atoms are summarized in Table S13 in the Supporting Information. These results indicate that the K, Rb, Cs, Ca, Sr, Ba, C, O, and F atoms in these crystals are in oxidation states of +1, +1, +1, +2, +2, +2, +4, −2, and −1, respectively.

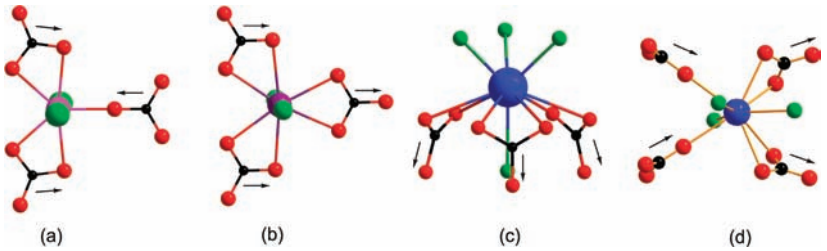

Figure 4. Alignments of CO_3 groups in alkaline−alkaline earth fluoride carbonates.

Table 2. Radius Ratio of Cations and NLO Effects of Alkaline−Alkaline Earth Fluoride Carbonates

crystals	radius ratio of cations (A^+/B^{2+})	SHG coefficient (visible) (× KDP)[a]	SHG coefficient (UV) (× BBO)[a]	geometric coefficient g	densities of the $[CO_3]$ (n/V) ($Å^{-3}$)	$(n/V) \times g$ ($Å^{-3}$)
$Cs_3Ba_4(CO_3)_3F_5$	1.157	1.20	0.33	0.45	0.00686	0.00307
$KSrCO_3F$	1.207	3.33	0.72	1	0.00889	0.00889
$RbSrCO_3F$	1.264	3.33	0.65	1	0.00858	0.00858
$KCaCO_3F$	1.341	3.61	0.74	1	0.00998	0.00998
$RbCaCO_3F$	1.525	1.11	0.24	0.33	0.00921	0.00304
$CsCaCO_3F$	1.658	1.11	0.22	0.33	0.00882	0.00291

[a] d_{36} (KDP) = 0.39 pm/V, d_{22} (BBO) = 2.2 pm/V.

3.3. Effect of Cations on Alignment of CO_3 in the Fluoride Carbonates. It is interesting that there are three different spatial arrangements for the common $[CO_3]$ triangles in the structure of these six alkaline−alkaline earth fluoride carbonates: (1) all the $[CO_3]$ groups align coparallel in $KSrCO_3F$, $RbSrCO_3F$, and $KCaCO_3F$ with an acentric space group of $P\bar{6}m2$; (2) two-thirds of the $[CO_3]$ groups are parallel and one-third are antiparallel in $RbCaCO_3F$ and $CsCaCO_3F$ with an acentric space group of $P\bar{6}2m$; (3) all the $[CO_3]$ groups incline to the $a-b$ plane by an angle in $Cs_3Ba_4(CO_3)_3F_5$ with an acentric space group of $P6_3mc$. The different connection modes of the building blocks could be attributed to the size of the different countercations.

There are two kinds of cations in these six crystals: alkali metals (K^+, Rb^+, Cs^+) and alkaline earth cations (Ca^{2+}, Sr^{2+}, Ba^{2+}). Possessing more positive charges and smaller ionic radii, alkaline earth cations can more easily attract the negative charges of anionic $[CO_3]^{2-}$ groups, dominating the assembly of the anionic groups. When compared to the smaller Sr^{2+} and Ca^{2+}, the coordination number for Ba^{2+} is higher. Therefore, the complicated coordination environment of Ba atoms in $Cs_3Ba_4(CO_3)_3F_5$, which is up to 10-fold coordination, results in a noncoplanar alignment of Ba−O bond far away from the equatorial plane of the Ba atoms (Figure 4c and 4d). Consequently, the alignment of the $[CO_3]$ triangles is noncoplanar in the unit cell.

In the other carbonates containing smaller Sr or Ca countercations, the alkaline earth ions have lower coordination numbers (7- or 8-fold) and form polygonal bipyramids with all the O atoms lying in the equatorial plane, leading to the coplanar alignment of all $[CO_3]$ triangles. Although they are all coplanar, the orientations of the $[CO_3]$ triangles are different in these five carbonates, depending on the influence of their countercations. The ratios of ionic radii between alkali and alkaline earth metal for each carbonate are list in Table 2. They can be divided into two groups according to the ratios: 1.2 to 1.4 for the three isostructures of $KSrCO_3F$, $RbSrCO_3F$, and $KCaCO_3F$, and 1.5 to 1.7 for the two isostructures of $RbCaCO_3F$ and $CsCaCO_3F$. In the low ratio group, the alkaline earth ions are 8-fold coordinated and form $Sr(Ca)O_6F_2$ hexagonal bipyramids (Figure 4b). The hexagonal alignment of the six equatorial O atoms results in the symmetric alignment of three $[CO_3]$ groups that are oriented in the same direction. In contrast, the alkali metals are much larger in size than alkaline earth metals in the other group. Therefore, the alkali metals are more coordinated to O or F atoms, leading to lower coordination numbers such as the 7-fold coordination observed for CaO_5F_2 pentagonal bipyramids. The pentagonal alignment of the five equatorial O atoms results in the asymmetric alignment of three $[CO_3]$ groups, (Figure 4a) in which two of them are parallel to each other by sharing their edges with CaO_5F_2, while the remaining $[CO_3]$ group is antiparallel to the others and shares its corner with CaO_5F_2.

We found that the three different alignments among the $[CO_3]$ groups originated from the coordination behaviors of the countercations. We therefore proposed that the moderate size of the alkaline earth ions coupled with the balance between the size of the alkali and that of alkaline earth metal should promote coplanar and parallel arrangement of the $[CO_3]$ groups, leading to a large macroscopic nonlinearity that will be detailed in next section.

3.4. Optical Properties. UV−vis diffuse reflectance spectra were collected for all of the reported compounds (see Figure S3 in the Supporting Information). Absorption (K/S) data were calculated from the following Kubelka−Munk function: $F(R) = (1 - R)^2/2R = K/S$, where R is the reflectance, K is the absorption, and S is the scattering. In the (K/S)-versus-E plots, extrapolating the linear part of the rising curve to zero provided the onset of absorption. No obvious absorption peak in the range of 6.22−1.55 eV (corresponding to 200−800 nm) was observed for $KSrCO_3F$, $RbSrCO_3F$, $KCaCO_3F$, $RbCaCO_3F$, and $CsCaCO_3F$, except for $Cs_3Ba_4(CO_3)_3F_5$ with a UV cutoff at ~210 nm, indicating that all of these crystals may have potential use in UV NLO applications.

The curves of the SHG signal as a function of particle size of the ground $KSrCO_3F$ crystals measured with a laser at 1064 and 532 nm as the fundamental waves are shown in Figure 5. A KDP

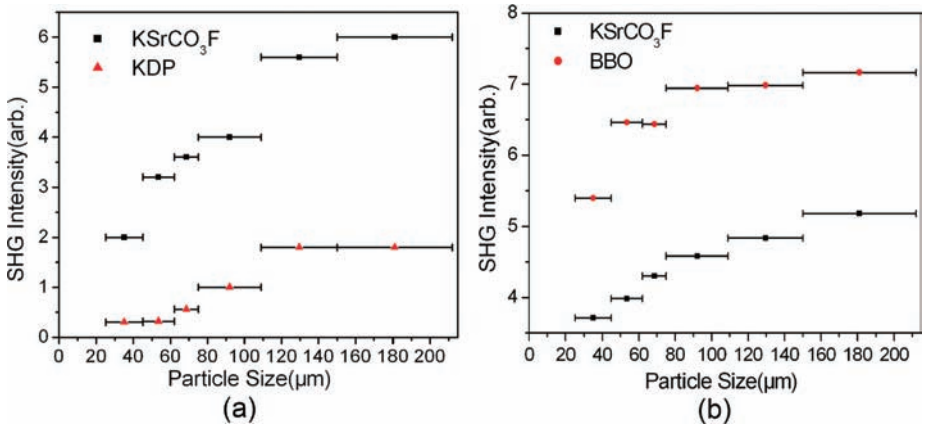

Figure 5. SHG measurements of ground $KSrCO_3F$ crystals (solid circle) and KDP (open circle) as the reference with the laser at 1064 nm wavelength (a), and SHG measurements of ground $KSrCO_3F$ crystals (solid circle) and BBO (open circle) as the reference with the laser at 532 nm wavelength (b).

sample was used as the reference for visible SHG, and BBO was used for UV SHG. The results are consistent with phase-matching behavior in both visible and UV region according to the rule proposed by Kurtz and Perry.[46] The SHG signal of the other five carbonates were measured only with the samples having a particle size around 100 μm, because we have not obtained enough crystals currently. The SHG measurement results for the six carbonates are list in Table 2. The relative magnitude of SHG coefficients in the visible region and those in the UV region are in accordance with each other, considering the NLO coefficient of BBO is about 5.6 times as large as d_{36} (KDP) which is 0.39 pm/V.[51]

On the basis of the anionic group theory,[52] the dipole transition from the cations to the anionic groups ($[CO_3]$ in this case) is the off-site transition. Its value is about 1 order smaller than the dipole transition of the intraatomic transitions within anionic groups. So the contribution to the main SHG coefficients from the anionic group $[CO_3]$ is dominant, which is much larger than that of the charge transfer between the s-states of cations and the p-originated states of anions. Therefore the macroscopic second-order susceptibility $\chi^{(2)}$ may be expressed by eq 2 according to the anionic group theory,

$$x_{ijk}^{(2)} = \frac{F}{V}\sum_{P}\sum_{i'j'k'}\alpha_{ii'}\alpha_{jj'}\alpha_{kk'}\beta_{i'j'k'}^{(2)}(P) \qquad P = [CO_3] \qquad (2)$$

where F is the correction factor of the localized field, $\alpha_{ii'}$, $\alpha_{jj'}$, and $\alpha_{kk'}$ are the direction cosines between the macroscopic coordinates of the crystal and the microscopic coordinates of $[CO_3]$ groups, i.e., the geometrical factor, and $\beta_{i'j'k'}^{(2)}$ are the microscopic second-order susceptibility tensors of the $[CO_3]$ group. Owing to the high symmetry of the crystal structure and the $[CO_3]$ group, eq 2 may be simplified according to the deduction process shown in ref 53:

$$d = F \times (n/V) \times g \times \beta_{111}([CO_3]) \qquad (3)$$

Assuming the equal localized field (F) based on their similar refractive index, the NLO coefficient d is proportional to density of the $[CO_3]$ group (n/V) and the geometric factor (g). Because the density of $[CO_3]$ groups is approximately equal for all cases except for $Cs_3Ba_4(CO_3)_3F_5$, the overall nonlinearity highly depends on the alignment of the $[CO_3]$ groups, which is expressed as the geometric factor g. When all the $[CO_3]$ groups are aligned coplanar, the calculation of g factor is quite straightforward. In the case of $KSrCO_3F$, $RbSrCO_3F$, and $KCaCO_3F$, the $[CO_3]$ triangles are all exactly parallel to each other, giving a 100% optimum. For $RbCaCO_3F$ and $CsCaCO_3F$, one-third of the $[CO_3]$ triangles are antiparallel to the others and results in a g value of 33%. On the other hand, the $[CO_3]$ triangles in $Cs_3Ba_4(CO_3)_3F_5$ are noncoplanar but oriented approximately to the c axis at an angle. The g factor can be calculated according to the relationship between the macroscopic and the microscopic coordinate systems by using eqs 2 and 3, which is 45%. As shown in Table 2, the above argument on structure−properties correlations is in good agreement with the SHG measurements.

4. CONCLUSIONS

A new series of alkaline−alkaline earth fluoride carbonates ($KSrCO_3F$, $RbSrCO_3F$, $RbCaCO_3F$, $CsCaCO_3F$, and $Cs_3Ba_4(CO_3)_3F_5$) were synthesized by incorporating halide anions into the carbonate system. $KSrCO_3F$ and $RbSrCO_3F$ are congruently melting compounds. These novel carbonate crystals were obtained by spontaneous crystallization with molten flux based on the self-fluxed system. The UV−vis diffuse reflectance spectroscopy study of powder samples indicated that the short-wavelength absorption edges of these materials are all below 200 nm, except for $Cs_3Ba_4(CO_3)_3F_5$ at ~210 nm. These crystals are all noncentrosymmetric. All of these crystals except $Cs_3Ba_4(CO_3)_3F_5$ are stacked by alternating $[AF]_\infty$ (A = K, Rb, Cs) and $[B(CO_3)]_\infty$ (B = Ca, Sr) layers, which are bridged via infinite B−F−B (B = Ca, Sr) chains parallel to the c-axis. The $[CO_3]$ group is the only NLO-active unit in these compounds. The different alignments of the $[CO_3]$ groups were found to be directed by the coordination behaviors of the countercations, which yielded different NLO nonlinearity for each carbonates. The SHG results indicated that $KSrCO_3F$, $RbSrCO_3F$, $KCaCO_3F$, $RbCaCO_3F$, $CsCaCO_3F$, and $Cs_3Ba_4(CO_3)_3F_5$ are all phase-matchable materials in both visible and the UV region, with measured SHG coefficients of about 3.33, 3.33, 3.61, 1.11, 1.11, and 1.20 times as large as that of d_{36} (KDP), respectively. These crystals are all stable in air and not hydroscopic, except for $Cs_3Ba_4(CO_3)_3F_5$. These features make the alkaline−alkaline earth fluoride carbonates very promising as UV NLO materials for practical applications. Furthermore, the discovery of new series of fluoride carbonate complex salts added CO_3-based compounds to the family of UV NLO materials.

■ ASSOCIATED CONTENT

Supporting Information. DTA traces, PXRD patterns, diffuse reflectance absorption curves, and crystal data (CIF). This material is available free of charge via the Internet at http://pubs.acs.org.

■ AUTHOR INFORMATION

Corresponding Author
nye@fjirsm.ac.cn

■ ACKNOWLEDGMENT

This work was supported by the National Science Foundation of China (nos. 50872132 and 90922035). The authors thank X. Y. Chen for the measurements of the powder SHG in the UV region.

■ REFERENCES

(1) Mei, L. F.; Wang, Y. B.; Chen, C. T. *Mater. Res. Bull.* **1994**, *29*, 81.
(2) Mei, L.; Huang, X.; Wang, Y.; Wu, Q.; Wu, B.; Chen, C. *Z. Kristallogr.* **1995**, *210*, 93.
(3) McMillen, C. D.; Kolis, J. W. *J. Cryst. Growth* **2008**, *310*, 2033.
(4) Chen, C. T.; Luo, S. Y.; Wang, X. Y.; Wang, G. L.; Wen, X. H.; Wu, H. X.; Zhang, X.; Xu, Z. Y. *J. Opt. Soc. Am. B* **2009**, *26*, 1519.
(5) McMillen, C. D.; Hu, J.; VanDerveer, D.; Kolis, J. W. *Acta Crystallogr., Sect. B: Struct. Crystallogr. Cryst. Chem.* **2009**, *65*, 445.
(6) Chen, C. T.; Wang, Y. B.; Wu, B. C.; Wu, K. C.; Zeng, W. L.; Yu, L. H. *Nature* **1995**, *373*, 322.
(7) Yang, Y; Pan, S. L; Li, H. Y; Han, J; Chen, Z. H; Zhao, W. W; Zhou, Z. D. *Inorg. Chem.* **2011**, *50*, 2415.
(8) Yang, Y; Pan, S. L; Han, J; Hou, X. L; Zhou, Z. X; Zhao, W. W; Chen, Z .H; Zhang, M. *Cryst. Growth Des.* **2011**, *11*, 3912.
(9) Wang, S. C.; Ye, N.; Li, W.; Zhao, D. *J. Am. Chem. Soc.* **2010**, *132*, 8779.
(10) Wu, H. P.; Pan, S. L.; Poeppelmeier, K. R.; Li, H. Y.; Jia, D. Z.; Chen, Z. H.; Fan, X. Y.; Yang, Y.; Rondinelli, J. M.; Luo, H. S. *J. Am. Chem. Soc.* **2011**, *133*, 7786.
(11) Wang, S. C.; Ye, N. *J. Am. Chem. Soc.* **2011**, *133*, 11458.
(12) Chang, H. Y.; Kim, S. H.; Halasyamani, P. S.; Ok, K. M. *J. Am. Chem. Soc.* **2009**, *131*, 2426.
(13) Chang, H. Y.; Kim, S. H.; Ok, K. M.; Halasyamani, P. S. *J. Am. Chem. Soc.* **2009**, *131*, 6865.
(14) Pan, S.; Smit, J. P.; Watkins, B.; Marvel, M. R.; Stern, C. L.; Poeppelmeier, K. R. *J. Am. Chem. Soc.* **2006**, *128*, 11631.
(15) Nguyen, S. D.; Yeon, J; Kim, S. H.; Halasyamani, P. S. *J. Am. Chem. Soc.* **2011**, *133*, 12422.
(16) Sun, C. F.; Hu, C. L.; Xu, X.; Ling, J. B.; Hu, T.; Kong, F.; Long, X. F.; Mao, J. G. *J. Am. Chem. Soc.* **2009**, *131*, 9486.
(17) Keszler, D. A. *Curr. Opin. Solid State Mater. Sci.* **1999**, *4*, 155.
(18) Ghotbi, M.; Ebrahim-Zadeh, M.; Majchrowski, A.; Michalski, E.; Kityk., I. V. *Opt. Lett.* **2004**, *29*, 2530.
(19) Ghotbi, M.; Sun, Z.; Majchrowski, A.; Michalski, E.; Kityk., I. V. *Appl. Phys. Lett.* **2006**, *89*, 173124.
(20) Chen, C. T.; Wu, B. C.; Jiang, A. D.; You, G. M. *Sci. Sin., Ser. B* **1985**, *28*, 235.
(21) Chen, C. T.; Wu, Y. C.; Jiang, A. D.; Wu, B. C.; You, G. M.; Li, R. K.; Lin, S. J. *J. Opt. Soc. Am. B* **1989**, *6*, 616.
(22) Wu, Y. C.; Sasaki, T.; Nakai, S.; Yokotani, A.; Tang, H. G.; Chen, C. T. *Appl. Phys. Lett.* **1993**, *62*, 2614.
(23) Mori, Y.; Kuroda, I.; Nakajima, S.; Sasaki, T.; Nakai, S. *Appl. Phys. Lett.* **1995**, *67*, 1818.
(24) Tu, J. M.; Keszler, D. A. *Mater. Res. Bull.* **1995**, *30*, 209.
(25) Mei, L.; Wang, Y.; Chen, C.; Wu., B. *J. Appl. Phys.* **1993**, *74*, 7014.
(26) Hu, Z. G.; Higashiyama, T.; Yoshimura, M.; Yap, Y. K.; Mori, Y.; Sasaki., T. *Jpn. J. Appl. Phys.* **1998**, *37*, 1093.
(27) Komatsu., R. *Appl. Phys. Lett.* **1997**, *70*, 3492.
(28) Grice Joel, D; Maisonneuve, V.; Leblanc, M. *Chem. Rev.* **2007**, *107*, 114.
(29) Mercier, N.; Leblanc, M.; Durand, J. *Eur. J. Solid State Inorg. Chem.* **1997**, *34*, 241.
(30) Mercier, N.; Leblanc., M. *Eur. J. Solid State Inorg. Chem.* **1993**, *30*, 217.
(31) Mercier, N.; Leblanc., M. *Eur. J. Solid State Inorg. Chem.* **1994**, *31*, 423.
(32) Park, H.; Barbier., J. *J. Solid State Chem.* **2000**, *155*, 354.
(33) Ben Ali, A.; Maisonneuve, V.; Smiri, L. S.; Leblanc., M. *Solid State Sci.* **2002**, *4*, 891.
(34) Ben Ali, A.; Maisonneuve, V.; Kodjikian, S.; Smiri, L. S.; Leblanc., M. *Solid State Sci.* **2002**, *4*, 503.
(35) Mercier, N.; Leblanc, M.; Antic-Fidancev, E.; Lemaître-Blaise, M.; Porcher., P. *J. Alloys Compd.* **1995**, *225*, 198.
(36) Antic-Fidancev, E.; Lemaître-Blaise, M.; Porcher, P.; Mercier, N.; Leblanc., M. *J. Solid State Chem.* **1995**, *116*, 286.
(37) Antic-Fidancev, E.; Corbel, G.; Mercier, N.; Leblanc., M. *J. Solid State Chem.* **2000**, *153*, 270.
(38) Chen, X. L.; He, M.; Xu, Y. P.; Li, H. Q.; Tu, Q. Y. *Acta Crystallogr., Sect. E: Struct. Rep. Online* **2004**, *60*, i50.
(39) Sun, Y. P.; Huang, Q. Z.; Wu, L.; He, M.; Chen, X. L. *J. Alloys Compd.* **2006**, *417*, 13.
(40) Halasyamani, P. S.; Poeppelmeier, K. R. *Chem. Mater.* **1998**, *10*, 2753.
(41) Ye, H.; Fu, D.; Zhang, Y.; Zhang, W.; Xiong, R. G.; Huang, S. D. *J. Am. Chem. Soc.* **2009**, *131*, 42.
(42) Sheldrick, G. M. *Acta Crystallogr., Sect. A: Found. Crystallogr.* **2008**, *64*, 112.
(43) Spek, A. L. *J. Appl. Crystallogr.* **2003**, *36*, 7.
(44) Kubelka, P.; Munk, F. Z. *Tech. Phys.* **1931**, *12*, 593.
(45) Tauc, J. *Mater. Res. Bull.* **1970**, *5*, 721.
(46) Kurtz, S. K.; Perry, T. T. *J. Appl. Phys.* **1968**, *39*, 3798.
(47) Lakshminarayana, G.; Kapustianyk, V.; Ozga, K.; Rudyk, V.; Kityk, I. V.; Brik, M. G.; Berdowski, J.; Tylczynski, Z. *Appl. Phys. A: Mater. Sci. Process.* **2011**, *104*, 721.
(48) Li, R. K.; Chen, P. *Inorg. Chem.* **2010**, *49*, 1561.
(49) Brown, I. D.; Altermatt, D. *Acta Crystallogr., Sect. B: Struct. Crystallogr. Cryst. Chem.* **1985**, *41*, 244.
(50) Brese, N. E.; O'Keeffe, M. *Acta Crystallogr., Sect. B: Struct. Crystallogr. Cryst. Chem.* **1991**, *47*, 192.
(51) Eckardt, R. C.; Masuda, H.; Fan, Y. X.; Byer, R. L. *IEEE J. Quantum Electron.* **1990**, *26*, 922.
(52) Chen, C.; Lin, C.; Wang., Z *Appl. Phys. B: Laser Opt.* **2005**, *80*, 1.
(53) Ye, N; Chen, Q. X; Wu, B. C; Chen, C. T. *J. Appl. Phys.* **1998**, *84*, 1.